Interpixel capacitance in non-destructive focal plane arrays

Andrew C. Moore,[a,b] Zoran Ninkov,[a] and William J. Forrest[b]

[a]Rochester Institute of Technology, Rochester, NY, USA
[b]University of Rochester, Rochester, NY, USA

ABSTRACT

Inter-pixel capacitive coupling can exist in a non-destructive detector array if the detector nodes change voltage as they integrate charge and the design of the device allows for an electric field to exist between adjacent collection nodes. Small amounts of inter-pixel capacitance can cause large errors in the measurement of poissonian noise versus signal, and all subsequently derived measurements such as nodal capacitance and quantum efficiency. Crosstalk and MTF can also be significantly influenced by interpixel capacitance. Two $1k \times 1k$ Raytheon SB226-based hybridized silicon PIN arrays were tested for nodal capacitance and MTF. Initial results indicated unexpected and unexplainably large nodal capacitance, poor MTF, and odd edge spread. It was hypothesized that inter-pixel capacitive coupling was responsible for these discrepancies. A stochastic method of measuring the coupling using 2D autocorrelation and Fourier Transform techniques was devised and implemented. Autocorrelation of the shot noise in the images revealed a correlation consistent with 3.2% interpixel capacitive coupling. When the effects of the measured interpixel capacitance were taken into account, the initially measured nodal capacitance of 56 fF was found to be 30% higher than the corrected nodal capacitance measurement of 43 fF. Large discrepancies between the theoretical and observed edge spread response were also greatly reduced. A simulation of the electric field in the PIN detector intrinsic region predicted an interpixel coupling very close to the observed coupling. Interpixel capacitance was also observed in $2k \times 2k$ Raytheon SB304-based InSb detector arrays, but was not strongly evident in a bare Raytheon SB226 multiplexer.

Keywords: Astronomical Imagers, CMOS Imagers, PIN array, MTF, interpixel capacitance

1. INTRODUCTION

In a previous paper, Moore *et al.*[1] recently suggested that inter-pixel capacitance can create significant errors in the "noise squared versus signal" method of estimating nodal capacitance,[2] and presented data supporting this suggestion. In this paper, the effects of inter-pixel capacitance and the mechanisms which cause them are investigated in more detail. Inter-pixel capacitance causes Poissonian noise in a device to appear lower than it actually is. As a result, the responsive quantum efficiency (RQE) is *overestimated* — the detector array appears to be collecting more photons than it actually is. For scientific detector arrays in low-signal applications such as space telescopes, the RQE of the array is the "bottom line" of its information-gathering ability — arrays with poor RQE take longer to accumulate the same information, and are proportionally that much more "expensive" to operate in order to make the same scientific discoveries. Crosstalk of 1% or more to neigboring pixels, observable in either hot pixels or cosmic events, may be a warning sign that actual RQE is *significantly poorer* than reported RQE determined from noise squared versus signal methods.

Inter-pixel capacitance is expected to become more significant with modern arrays. As photodetector array designers continue to strive for the simultaneous qualities of high pixel density (requiring small distances between pixel centers) high quantum efficiency and low latent images (requiring 100% fill factor — small gaps betweeen pixel implants) and high sensitivity (low capacitance detection nodes) the stray capacitance to neighboring pixels will be more pronounced. Stray capacitance to a detector node is from the presence of conductors adjacent to the detector node. Detector nodes must be conductive in order to reflect a voltage from accumulated charge. Thus, the nearest conductors adjacent to the pixels in the lowest capacitance detector arrays will be the neighboring pixels.

Further author information:
E-mail: andrew.moore@rochester.edu

Focal Plane Arrays for Space Telescopes, edited by Thomas J. Grycewicz, Craig R. McCreight,
Proceedings of SPIE Vol. 5167 (SPIE, Bellingham, WA, 2004)
0277-786X/04/$15 · doi: 10.1117/12.507330

2. BASIC MECHANISM

A photodetector array of the type considered here may be modeled as an array of capacitors $C_{i,j}$, each receiving a signal $\bar{Q}_{i,j}$. The bar indicates that the charge is the accumulated photocurrent *entering* node i,j over some time t:

$$\bar{Q}_{i,j} = \int_{\tau=0}^{\tau=t} I_{i,j}(\tau)\, d\tau \tag{1}$$

The output of the array is ideally a voltage $V_{i,j}$ such that

$$V_{i,j} = \frac{\bar{Q}_{i,j}}{C_{i,j}}. \tag{2}$$

This is a simplification in several respects. Pixels are frequently non-linear — the capacitance changes with voltage. This non-linearity may be ignored in the analysis that follows as the stochastic signal considered (the Poissonian noise) is very small. Pixel non-linearity can also cause significant error in measurement of conversion factor.[3]

Typically, all capacitors $C_{i,j}$ are (roughly) equal by fabrication, and the subscript i,j is omitted from C. There are, however, slight variations in nodal capacitance — also ignored here.

Equation 2, although very simple, has been the nodal electrical model to date. Crosstalk in detector arrays (and systems) from various other sources has been considered.[4,5,6,7,8,9] The optical system's PSF frequently contributes crosstalk to observed results, and must be distinguished from that of the array. "Optical crosstalk" (reflection of light within the detector) may also be significant if penetration depth is large. Crosstalk from diffusion of carriers, referred to in several of these references as "electrical crosstalk," is considered most frequently. Inter-pixel capacitance provides a new "electrical crosstalk" mechanism. With the previous simplifications, the array can be modeled as a discrete linear shift-invariant[10] (LSI) system, outputting an array of voltages:

$$V_{i,j} = \sum_{m=-\infty}^{\infty} \sum_{n=-\infty}^{\infty} \bar{Q}_{m,n} h(i-m, j-n) = \bar{Q}_{i,j} * h(i,j). \tag{3}$$

where $*$ is the 2D convolution operator. Ideally,

$$h(i,j) = \frac{\delta(i,j)}{C_{node}}. \tag{4}$$

where $\delta(i,j)$ is the discrete 2D "unit impulse" or "delta function".

An equivalent continuous representation of the discrete array,

$$g(x,y) = \sum_{i=-\infty}^{i=\infty} \sum_{j=-\infty}^{j=\infty} g(i,j)\, \delta(x-i)\, \delta(y-j). \tag{5}$$

where $\delta(x,y)$ is the continuous 2D impulse function, is substituted where convenient in the analysis that follows.

Inter-pixel capacitance is modeled as small coupling capacitors between detector nodes, as shown in Figure 1. Photocurrent into a single detector node returns via multiple paths. Using Kirchoff's current law, it can be seen that the total charge entering the single node (at the top of Figure 1) is equal to the total charge appearing electrically on that node's voltage V and its neighbors,

$$\bar{Q} = \int_{\tau=0}^{\tau=t} I(\tau)\, d\tau = \int_{\tau=0}^{\tau=t} \sum_n I_n(\tau) d\tau = \sum_n \int_{\tau=0}^{\tau=t} I_n(\tau)\, d\tau = \sum_n Q_n. \tag{6}$$

where I_n is the current through the n_{th} nodal capacitance and Q_n is the charge appearing electrically on that capacitance.

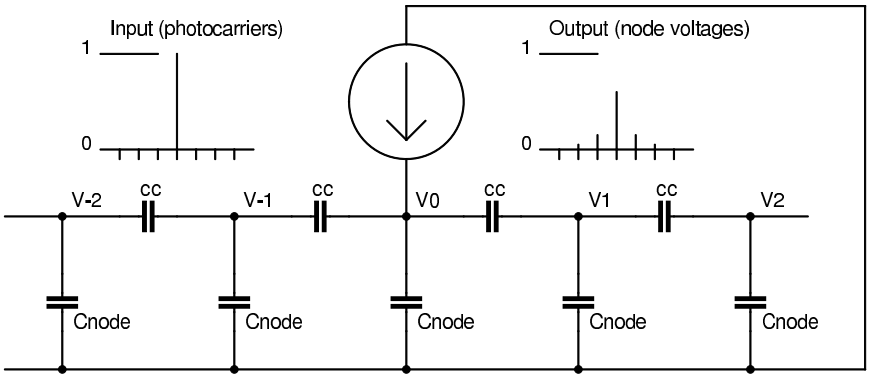

Figure 1. By Kirchoff's current law, the current entering the single node at the top is the sum of all the currents leaving all of the nodes at the bottom.

Thus,

$$\sum_n V_n = \sum_n \frac{Q_n}{C_{node}} = \frac{\sum\limits_n Q_n}{C_{node}} = \frac{\bar{Q}}{C_{node}}. \tag{7}$$

and the photocarriers collected in a single node appear upon readout to be distibuted into several nodes, but only the nodal capacitance C_{node} appears in the "DC" output of the detector array. The impulse response of the detector nodes in this one-dimensional model is

$$h(n) = \frac{Q_n}{\bar{Q} C_{node}}. \tag{8}$$

This readily applies to a two dimensional array; the nature of the network of coupling capacitors in Figure 1 is unimportant with respect to Kirchoff's current law and could just as easily have been a "black box."

It is convenient to normalize out the nodal capacitance using $C_{node} = 1$, and express the impulse response such that it represents a deviation from the ideal response. Thus,

$$h(i,j) = \frac{\int\limits_{\tau=0}^{\tau=t} I_{i,j}(\tau)\, d\tau}{\int\limits_{\tau=0}^{\tau=t} I_{src}(\tau)\, d\tau}. \tag{9}$$

and

$$\sum_{i=-\infty}^{i=\infty} \sum_{j=-\infty}^{j=\infty} h(i,j) = 1. \tag{10}$$

It can additionally be noted that

$$h(i,j) \geq 0. \tag{11}$$

since inter-pixel capacitance pulls the voltages of neighboring nodes in the same direction, and

$$h(i,j) \leq 1. \tag{12}$$

as the circuit is passive and cannot create an output greater than its input. Symmetry is reasonable to assume.

$$h(i,j) = h(-i,-j). \tag{13}$$

There is strong evidence that inter-pixel capacitive coupling is not symmetrical around defective ("hot") pixels in InSb arrays. Normal pixels are likely have slight variations as well, but the average coupling is symmetrical.

3. RESPONSE TO POISSONIAN NOISE

Photocurrent arrives in detector nodes quantized by the charge of an electron. Photon arrival and diffusion in the detector are both stochastic processes, and without correlation mechanisms in photon arrival and diffusion,* the individual collection events may be assumed statistically independent. Thus, charge collected by detector nodes may be expressed as a mean signal component $M_{i,j}$ plus a "white" noise image $N_{i,j}$

$$\bar{O}_{i,j} = M_{i,j} + N_{i,j}. \tag{14}$$

The white noise image has a uniform power spectral density S_N,

$$S_N(\xi,\eta) = \lim_{T\to\infty} \frac{E\left\{|\mathscr{F}\{N_{i,j}\}|^2\right\}}{2T} = \lim_{T\to\infty} \frac{E\left\{|F_N(\xi,\eta)|^2\right\}}{2T} = \sigma_N^2. \tag{15}$$

where $E\{\}$ is the expectation operator, $\mathscr{F}\{\}$ is the Fourier transform operator resulting in $F_N(\xi,\eta)$, and ξ and η are spatial frequency (x and y) in cycles per pixel. The inter-pixel capacitive impulse response $h(i,j)$ causes the output to differ from this white charge collected by the detector nodes. The observed voltage output is:

$$V_{i,j} = \frac{M_{i,j} + N_{i,j}}{C_{node}} * h(i,j). \tag{16}$$

In the absence of a gain mechanism, i.e., assuming one electron per photon, the variance of the noise image σ_N^2 is equal (in quanta) to the mean signal M.

The difference $D_{i,j}$ of a pair of identically acquired images V^1 and V^2 results in a noise image that is twice the variance of the original images' noise components. The difference cancels out the signal component, leaving only the noise:

$$D_{i,j} = V_{i,j}^1 - V_{i,j}^2 = \frac{N_{i,j}^1 - N_{i,j}^2}{C_{node}} * h(i,j). \tag{17}$$

which is typically compared to the mean of the sum of the images to obtain an estimate of the conversion factor. Uniform illumination $M_{i,j} = M$ is typically used, but has not been assumed yet. If the noise difference image can be considered a stationary 2D random process, (this covers random spatial variations in illumination and pixel response) the power spectral density of the noise image in Equation 17 is

$$S_D(\xi,\eta) = \lim_{T\to\infty} \frac{E\left\{|\mathscr{F}\{D_{i,j}\}|^2\right\}}{2T} = 2\lim_{T\to\infty} \frac{E\left\{|F_N(\xi,\eta)\,H(\xi,\eta)|^2\right\}}{2T} = 2\sigma_N^2 |H(\xi,\eta)|^2. \tag{18}$$

Thus, the power spectral density of the observed difference image yields information about the inter-pixel capacitive effect. Since the input signal (the noise on the charge collected by the nodes) is white, the output spectrum is proportional to the squared magnitude of the Fourier transform of the impulse response.

Direct measurement of the power spectra of random processes is generally discouraged; autocorrelation techniques are preferred. The Weiner-Khinchine relation in two dimensions

$$S(\xi,\eta) = \int_{-\infty}^{+\infty}\int_{-\infty}^{+\infty} R(x,y)\, e^{-j2\pi\xi x} e^{-j2\pi\eta y} dx dy = \mathscr{F}\{R(x,y)\}. \tag{19}$$

expresses the power spectral density of a 2D random process in terms of its autocorrelation function. The power spectral density of a 2D stationary random process $S_V(\xi,\eta)$ is obtained by measuring its autocorrelation function $R_V(x,y)$, then taking the Fourier transform of that.

Combining Equations 18 and 19 results in:

$$\mathscr{F}\{R_D(x,y)\} = 2\sigma_N^2 |H(\xi,\eta)|^2. \tag{20}$$

*Known correlation mechanisms in photon arrival (such as Hanbury-Brown-Twiss) and diffusion (such as carrier-carrier interaction) seem unlikely to be significant here.

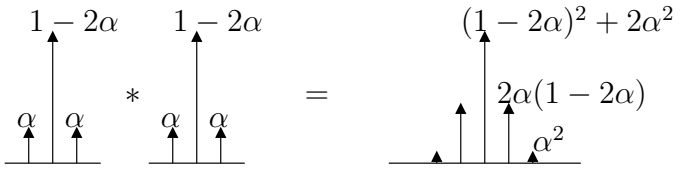

Figure 2. Convolution of 1D coupling impulse response with itself.

or, equivalently:

$$\mathscr{F}\left\{R_D\left(x,y\right)\right\} = 2\sigma_N^2 \left|\mathscr{F}\left\{h\left(x,y\right) * h\left(x,y\right)\right\}\right|. \tag{21}$$

Since $h\left(x,y\right)$ is non-negative and even, no phase information is actually removed by the magnitude operator and

$$\frac{\mathscr{F}\left\{R_D\left(x,y\right)\right\}}{2\sigma_N^2} = \left(\mathscr{F}\left\{h\left(x,y\right)\right\}\right)^2. \tag{22}$$

Taking the inverse Fourier transform of Equation 22 yields

$$\frac{R_D\left(x,y\right)}{2\sigma_N^2} = h\left(x,y\right) * h\left(x,y\right). \tag{23}$$

and the normalized autocorrelation is equal to the convolution of the impulse response with itself. Taking the square root of Equation 22 first (this can be done here since $h\left(x,y\right)$ and $H\left(\xi,\eta\right)$ are both even and non-negative) and then taking the inverse Fourier transform results in

$$\mathscr{F}^{-1}\left\{\left[\frac{\mathscr{F}\left\{R_D\left(x,y\right)\right\}}{2\sigma_N^2}\right]^{\frac{1}{2}}\right\} = h\left(x,y\right). \tag{24}$$

This is a direct expression which may be used to obtain the impulse response of inter-pixel capacitance from the autocorrelation of the shot noise in a difference image.

The total power of the output power spectral density in Equation 18 is the mean square output, and by Parseval's relation, is:

$$\overline{D^2} = R_D\left(0,0\right) = 2\sigma_N^2 \int_{-\infty}^{+\infty}\int_{-\infty}^{+\infty} \left|H\left(\xi,\eta\right)\right|^2 d\eta d\xi = 2\sigma_N^2 \sum_{i=-\infty}^{+\infty}\sum_{j=-\infty}^{+\infty} h^2\left(i,j\right). \tag{25}$$

Thus, the sum of the squares of the impulse response is the gain factor of the white input noise variance caused by the inter-pixel capacitance. This gain factor is always less than or equal to one.

Since the impulse response $h\left(i,j\right)$ has unit area, its convolution with itself does also, and the summation of Equation 23 results in:

$$\sum_{i=-\infty}^{+\infty}\sum_{j=-\infty}^{+\infty} R_D\left(i,j\right) = 2\sigma_N^2. \tag{26}$$

This is a direct expression for the shot noise collected by the input nodes, and may be used to estimate "noise squared" in lieu of the frequently applied (and now incorrect) variance estimator

$$\widehat{R}_D\left(0,0\right) = \widehat{\overline{D^2}} = \frac{\sum\limits_{i,j}\left(D_{i,j}\right)^2}{N-1}. \tag{27}$$

which does not account for inter-pixel coupling.

Figure 2 illustrates the convolution of Equation 23 in one dimension. For simplicity, the "second neighbor" coupling is assumed to be zero. Since the center node loses α of its charge to each of its two neighbors, its

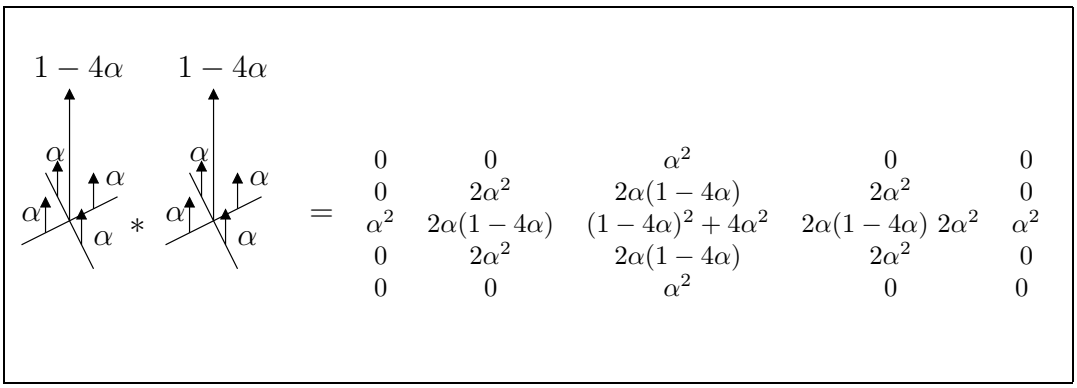

Figure 3. Convolution of 2D coupling impulse response with itself.

response is low by 2α. If α is small, $1-2\alpha \approx 1$ and the nearest-neighbor coefficient in the convolution result is $R(1) \approx 2\alpha$. In two dimensions, neglecting "second neighbor" and "diagonal neighbor" coupling, the center node loses 4α of its charge, α to each of its four nearest neighbors, and the resulting convolution is shown in Figure 3.

The center term of the convolution, $R(0,0)/2\sigma_N^2 = \overline{h^2} \approx (1-4\alpha)^2 \approx 1-8\alpha$, also expressed in Equation 25, is the relative mean square output of the noise compared to what would be measured without any inter-pixel coupling — the factor by which conversion gain is in error when inter-pixel capacitance is significant. The approximation $1-8\alpha$ holds for small amounts of coupling, and illustrates the magnitude of error this effect can cause. 1.25% coupling to a neighbor can cause a 10% error in estimated conversion factor.

4. INTER-PIXEL CAPACITANCE AND DETECTIVE QUANTUM EFFICIENCY.

The true measure of a detector array's performance is its detective quantum efficiency (DQE.) DQE is the squared SNR at the output of the array compared to the squared SNR incident at the surface of the array. Shaw[11] generalized the definition of DQE for imaging application to include a spatial frequency dependence. Stochastic scattering from diffusion reduces DQE at high spatial frequencies,[7] and in an otherwise perfect detector, DQE is reduced by the square of $T(\omega) = T(2\pi\xi)$, the scattering MTF:

$$DQE(\omega) = |T(\omega)|^2. \tag{28}$$

In fully depleted arrays such as the Si PIN device shown in Figure 5, stochastic scattering leads to a Gaussian scattering MTF. In detectors with "per-pixel" depletion regions as shown in Figure 4, such as the InSb devices treated later, the MTF is approximately:[12]

$$T(\omega) = \frac{2e^{-\omega}}{1+e^{-2\omega}}. \tag{29}$$

where ω is the spatial frequency in radians per thickness of the detector. (Thinner detectors have better MTF.)

Inter-pixel capacitance, like scattering, also reduces MTF, with a transfer function of approximately

$$T(\xi,\eta) = ((1-2\alpha) + 2\alpha\cos(2\pi\xi))\,((1-2\alpha) + 2\alpha\cos(2\pi\eta)). \tag{30}$$

for small α. Here, ξ and η are spatial frequency in cycles per pixel — the minimum MTF is at the Nyquist frequency of one cycle per two pixels. It is very easy to mistakenly attribute the effects of inter-pixel capacitive coupling to diffusion. Inter-pixel capacitance is a deterministic scattering mechanism however, and attenuates photon noise and signal identically at all spatial frequencies. Thus, inter-pixel capacitance has no effect upon *device* DQE, and its effect should be distiguished from diffusion MTF for the purpose of accurately evaluating $DQE(\omega)$ for an array. The inter-pixel capacitive effect *can* cause errors in the *measurement* of DQE, as it reduces the observed Poissonian noise and causes DQE to be overestimated the same way RQE is overestimated.

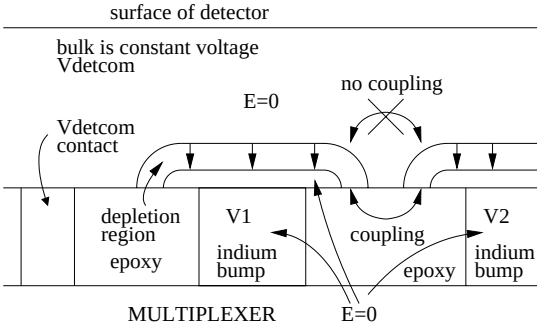

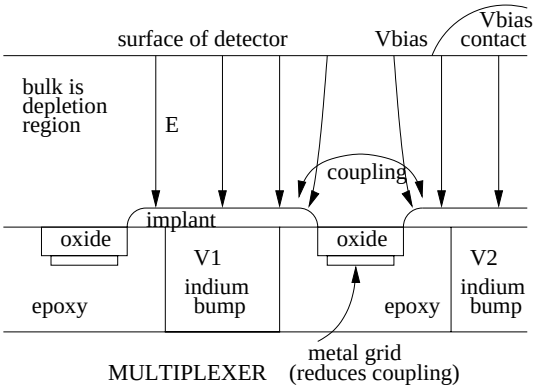

Figure 4. (Left) When the detector bulk is unbiased, inter-pixel capacitive coupling through the bulk is impossible. The insulating area below the implant allows the only coupling.

Figure 5. (Right) When the detector bulk is biased as in silicon PIN arrays, inter-pixel capacitive coupling through the bulk is possible. The insulating area below the implant allows additional coupling, but a " field control" grid between the pixels reduces coupling here.

5. MECHANISMS OF INTER-PIXEL CAPACITIVE COUPLING

In the previous paper,[1] it was suggested that the inter-pixel coupling mechanism was between the indium bumps. This hypothesis was incorrect. It is believed the coupling exists mainly through fringing fields between the edges of the pixel implants. As an illustration of this, two very different types of detector are considered here, which couple pixel-to-pixel with two different field paths. The first is a hybridized silicon PIN array for visible imaging, a detector with fully depleted bulk. The second is a hybridized indium antimonide array for infrared imaging, a "per-pixel" depleted detector.

The hybridized silicon PIN array, shown in Figure 5, is somewhat unusual — it operates with the detector bulk fully depleted, so electric fields exist throughout the bulk. A metal grid, deposited on thick oxide between the pixels, controls the electrical state of the silicon gap between the pixel implants. This voltage is biased to keep the gap out of both inversion and accumulation. The presence of this grid also (unintentionally) prevents significant inter-pixel coupling in the space between the indium bumps — it heavily influences the potential in this region where significant coupling otherwise would occur. It must do this, unfortunately, by increasing the nodal capacitance, and thus reducing sensitivity. Arsenic-doped silicon IBC detectors[13] (for 5-30 micron infrared) are similar to the silicon PIN arrays in that they are operated with partially or fully depleted bulk.

The indium antimonide array, depicted in Figure 4 is a more typical detector. The bulk is doped opposite that of the implants, and each pixel maintains a separate depletion region close to the pixel implant. The bulk of the detector, however, is conductive. No electric field, and therefore no inter-pixel capacitive coupling, can exist in the detector bulk. There is no metal grid controlling the surface state in the gaps between pixels in the illustration however, (although some per-pixel depleted arrays do have field control grids) and inter-pixel coupling can exist here. Mercury-Cadmium-Telluride detector arrays and others are typically similar to this.

A simulation of the potential between the pixels and the back bias surface of the PIN array was performed using a Python script employing the "numarray" Python module developed by Space Telescope Science Institute. A pixel-to-pixel spacing of 27 microns, detector thickness of 185 microns, and a gap of 5 microns (estimated) were used in the simulation. Detector node voltages were fixed at ground, and the back bias fixed at 30 volts. The intrinsic region was modeled as purely intrinsic. The potential at each point in a rectangular grid was iteratively solved for, and the electric field at the edge of the pixel implants was derived from these potentials. The center pixel was varied slightly, the potentials were readjusted, and fields re-derived. The results are shown in Figure 6.

The trace in Figure 6 with long dashes represents the field with all pixels at ground potential and the back bias at 30 volts. The area underneath this curve is proportional to the charge created by a 30 volt bias. Reducing

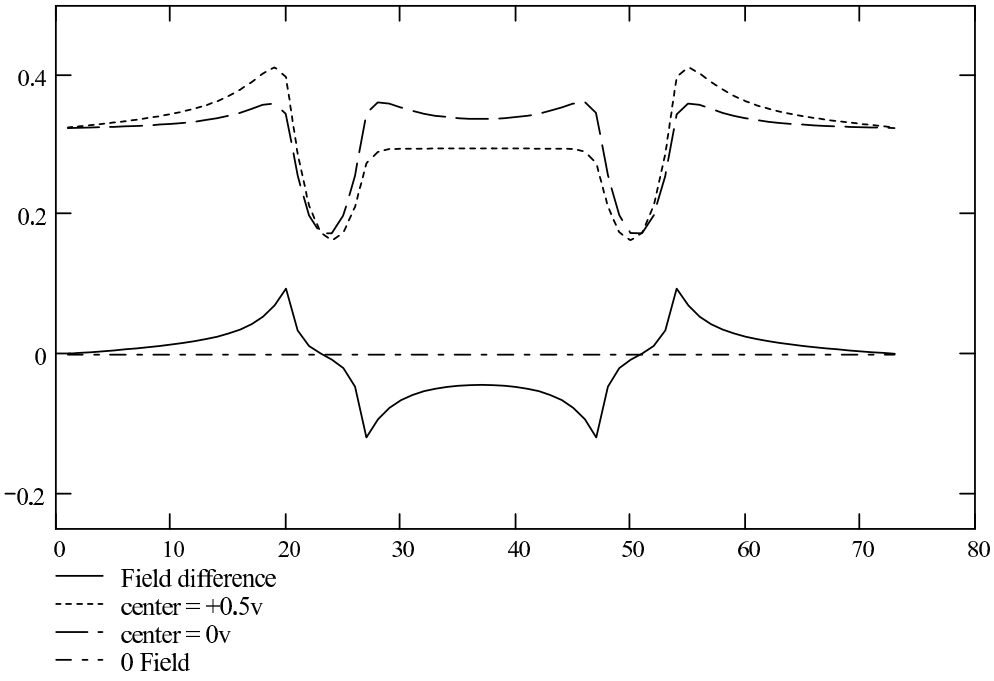

Figure 6. A simulation of the electric field in the bulk of the PIN detector with 30 volts of bias.

the bias on the center pixel by 0.5 V resulted in the trace with short dashes. A change in voltage of one-sixtieth of the back bias has caused the pixel to lose approximately one-sixth of its charge. Since the pixel's capacitance to the back bias is known from parallel plate calculation (and experiment) to be 0.25 fF, this implies approximately 2.5 fF of capacitance from the pixel to its two simulated neighbors. (Since the simulation was one-dimensional, its results are representative of the line response.) Doubling this result yielded an estimate of the coupling in the two-dimensional array.

6. INTER-PIXEL CAPACITANCE IN TESTED ARRAYS

The previous paper[1] detailed the evaluation of nodal capacitance and edge spread in silicon PIN arrays. This is reviewed briefly here, with some elaboration on initial expectations, the initially confusing measurements, and their ultimate explanation. New measurements on InSb arrays are also presented.

6.1. Expected PIN Nodal Capacitance and Edge Spread

The prototype silicon PIN detector arrays were expected to exhibit ultra-low nodal capacitance (33 fF), due to the large distance (185 microns) between their "parallel plates". The strong electric field in the depleted "i" region would rapidly sweep photocarriers into detector nodes (3 nanoseconds) and sharp imaging ($\approx 4\mu m$ diffusion spread) was anticipated. The overall point spread expected was the convolution of a 2D *gaus* and a 2D *rect*:

$$psf_{pixel}(x, y; b) = [rect(x)\, rect(y)] * gaus(x, y; b)\,. \tag{31}$$

Noise squared versus signal initially indicated 56 fF. Some of the extra capacitance was immediately accounted for — bias sensitivity tests indicated that approximately 18.3 percent of the total nodal capacitance was to the grid.

234	-5141	3731	-5354	-3304	3869	-3886	-5010	-661
295	2974	590	-6231	-1335	3484	117	-4145	4097
-1434	-4694	-574	16196	23060	5123	521	-1549	3556
-6783	-10180	9578	63021	253064	61183	12483	4232	-513
7065	-569	30770	258440	4044351	259273	30120	1392	7085
-1271	3493	12989	59031	252469	64626	11585	-10714	-9797
3915	-8	-83	5127	21765	16001	468	-6371	-5731
950	-3846	-671	6788	-3679	-8255	-80	-125	782
-1674	-2180	-4439	3440	-5133	-3676	1106	-4557	-105

Figure 7. Autocorrelation summation observed in silicon PIN array.

Edge spread testing used a sharp edge mask in direct contact with the array surface. The resulting edge spread did not fit the model well at all, but repeated attempts produced the same result, and the same spread was seen with long wavelength near IR and short wavelength blue.

Finally, the inter-pixel capacitance mechanism was considered, and it explained both observations.

6.2. Inter-pixel Capacitance Measurement in the PIN Array

The impulse response of the readout was measured by performing spatial autocorrelation of the Poissonian noise in 1800 multiply-sampled difference patches, 50 by 50 pixels in size. The raw results of this processing are shown in Figure 7. Then, making use of Equation 24, the 2D Fourier Transform of this autocorrelation was taken, each term in the transform was replaced by its square root, and the 2D inverse transform was normalized to a DC response of 1, yielding an estimate of the readout impulse response. The central value was estimated at 0.871, the four nearest neighbors were 0.027, and the four diagonal neighbors were 0.00525.

6.3. Inter-pixel Capacitance Measurement in the InSb Array

The University of Rochester Near Infrared Astronomy lab has been working with Raytheon on the development of indium antimonide infrared detector arrays.[14,15] A 2k × 2k SB304-based indium antimonide array from this program was measured for inter-pixel capacitance, and the resultant data are shown in Figure 8. A simpler method, illustrated in Figures 2 and 3 may be used to quickly estimate inter-pixel coupling from the autocorrelation data when the coupling is of this magnitude — simply compare half of a nearest neighbor autocorrelation coefficient to the central value. This quicker method is valid when the coupling to a nearest neighbor is 2.5 percent or less, as it assumes the central node is "near unity". These data show a coupling of roughly 1.4%, implying ≈ 11% error — an overestimation of RQE, DQE, and read noise. The inter-pixel capacitive effect in the InSb array is less than half that of the silicon PIN array. Since the dielectric constant of the epoxy in the InSb array is slighly less than half the dielectric of the Si of the PIN array, but the InSb pixels may be slightly closer together, this result makes some sense. However, slightly less coupling was observed in InSb cosmic ray data and leaky pixels, and the overall nodal capacitance of the PIN is smaller than that of the InSb, so less coupling was expected. As a control, a bare SB226 multiplexer was also tested for inter-pixel capacitive effects. A small amount appears to be present, however it is less than 0.5 % coupling. This makes sense too, as the dielectric constant of vacuum is a fraction of that of the epoxy or silicon. It does suggest that inter-pixel capacitive coupling might exist in monolithic CMOS arrays.

6.4. Corrections to the PIN models and measurements

With inter-pixel capacitance included, three components create the overall point spread function of the PIN device — diffusion in the detector, capture by square pixels, and inter-pixel capacitive effects. Only vertical and horizontal edges were used for evaluation, thus the expected ESF was the convolution of the readout's 1D impulse response, a 1D *rect* for the pixel, and an integrated Gaussian:

$$esf_{pixel}(x;b) = (0.0375 rect(x+1) + 0.925 rect(x) + 0.0375 rect(x-1)) * \int_0^x gaus(x';b)\,dx'. \qquad (32)$$

-2613	987	611	-638	-1	1175	514	1640	656
-559	-850	-580	-1537	-614	-228	-129	372	-111
-392	608	296	-441	-927	-1170	-242	536	-1336
1304	-252	-1186	1499	14341	2357	-482	513	-856
5773	-519	-187	15236	476374	15200	145	-319	6460
-645	682	-140	2609	14502	1173	-1015	-191	1426
-997	908	-191	-1373	-1295	-296	734	500	462
-664	-83	-600	-196	-1100	-1627	-274	-1190	-838
960	1335	257	1128	-430	-1311	687	678	-2203

Figure 8. Autocorrelation summation for InSb SB304-008.

-1593	-4527	-3370	-12992	-8465	-14391	-9011	5516	12837
6884	-11663	-14424	-25546	-9729	2488	1327	23931	-7725
13557	-2258	13176	12266	-14110	-3361	-7491	-3259	1982
-24251	-16350	-16225	15689	62767	8123	-5551	-24604	-10418
13391	-6480	2426	86357	9688799	83520	2417	-7187	11022
-20373	-15621	-951	6135	57246	13699	-9399	-23638	-19906
4898	2247	-7796	-1289	-11361	12583	7762	1506	8185
-15312	9330	-3371	5550	-21606	-25281	-9267	-4593	11049
11404	5356	-9924	-7959	-26880	-17879	-4174	-2917	898

Figure 9. Autocorrelation summation for bare SB226 multiplexer.

Figure 10 shows PIN edge spread data compared to two models — uncorrected and corrected. The dashed line is the original model that considered only diffusion and square pixels. It is the edge spread derived from the point spread of Equation 31. The solid line is the corrected model considering inter-pixel capacitance as well as a best-fit Gaussian spread, from Equation 32. This corrected model fits the data much better. (The same Gaussian spread was used in both models.)

For the conversion factor measurement, the effect of the readout response on the noise measurement must be considered. As shown in Equation 7 the signal component (low spatial frequency) is unaffected. This is not the case at high spatial frequencies, where most of the Poissonian noise image energy is. Using the relationship in Equation 25, the noise attenuation caused by inter-pixel capacitance was calculated:

$$\sum_{i,j} h^2\left(i,j\right) = 0.871^2 + 4\left(0.027^2 + 0.00525^2\right) = 0.762 = 1.313^{-1}. \tag{33}$$

Thus, an initally calculated conversion factor of $2.4e^-$/ADU was corrected to be $1.83e^-$/ADU and the nodal capacitance, previously 56 fF, was corrected to be 43fF. Responsive quantum efficiency measurements were taken using the (AR coated) PIN array, and are shown in Figure 11. RQE was near 90% at many wavelengths, a sensible result. Without inter-pixel compensation, this measurement would have been 117%, implying gain at photon energies where gain is known to be impossible.

7. A THIRD ELECTRICAL CROSSTALK — SETTLING TIME

An additional kind of "electrical crosstalk," in which a pixel value does not settle fully before it is sampled, can also affect noise squared versus signal measurements. Some evidence of this crosstalk can be seen in the first and last values of the middle row of Figure 8. The SB304, like the SB226, has four interleaved outputs, so the "next pixel" on any output is four columns over in the output image. If the output does not fully settle, a "fourth column" crosstalk will emerge in the autocorrelation. The other correlation arrays taken from the SB226 do not show this fourth column effect — The 1k × 1k SB226 has a smaller column bus capacitance than the 2k *times* 2k SB304 and settles faster. Also, the SB226 was operated in a system with only two A/D converters, and extra

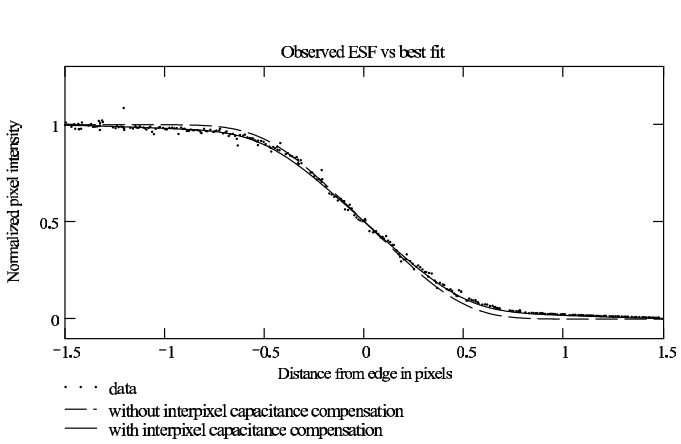

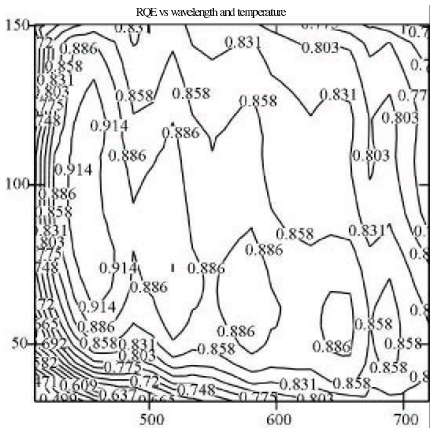

Figure 10. (Left) Edge spread in silicon PIN array, showing both original expected (uncorrected) and best-fit corrected models.

Figure 11. (Right) Responsive Quantum Efficiency in silicon PIN array, from 410 to 720 nm and 30 to 150K.

settling time was added for switching between the outputs. Hot pixel data from the SB304 did not seem to agree with the correlation data for fourth column crosstalk (hot pixels showed more crosstalk), but column bus settling is non-linear (eventually becoming slew rate limited) for larger signal swings, so this was not unexpected. In any event, incomplete settling — although controllable — is capable of creating additional error in the measurement of Poissonian noise.

8. DISCUSSION

Measuring conversion factor and nodal capacitance on CMOS imagers using noise-squared versus signal is a tricky business. Pain and Hancock's[3] method to address non-linear pixel response illustrates this as well. The error mechanism they address differs from the one addressed here, but there is a basic similarity — if the noise is measured using a different effective gain than the signal, the square of this gain error will appear in the conversion factor. Measuring the readout's impulse response by using autocorrelation requires care, as the correlation is very small compared to the Poissonian noise, let alone to the signal. Large amounts of data, a stable light source, multiple sampling, and cosmic ray rejection are all necessary. Adequate signal and multiple sampling to raise the shot noise above the read noise is desired. Excessive signal, however, brings the stability of the lamp into consideration. Long integration times stabilize some things, but make cosmic rays more likely; cosmic events can create large correlations, but are easily detected and rejected in most cases. Quantum gain can create correlation and should be avoided. It is desirable that the (uniform) image presented on the array be lacking in high spatial frequency content (a de-focused optical system is best) as vibration coupled with slight non-uniformities in the incoming optical signal may create some correlation in the output. The SB304 data were taken with a small aperture, and may have had some extra correlation introduced in this manner. The signal at high spatial frequencies is theoretically recoverable, but this recovery is more difficult if the detector is not uniform — characterization of the average coupling may be insufficient, and coupling may need to be measured independently for each pixel. Non-linearity of inter-pixel coupling (in non-PIN devices) is another issue. As pixels accumulate charge, the coupling to neighbors decreases with the increased gap.

9. SUMMARY

A mechanism that causes detector nodal voltages to differ from the charge collected by those same detector nodes, inter-pixel capacitance, is presented. Its specific mechanisms in both fully depleted and per-pixel depleted

arrays are investigated, and its effect on point spread and estimation of conversion factor are investigated. A technique for measurement of inter-pixel capacitance is presented and applied to real measurements on silicon PIN arrays, resulting in better agreement between models and observed data.

ACKNOWLEDGMENTS

Funding for researching improved operation and test of scientific detector arrays was provided by the Microelectronics Design Center (MDC) and the Center for Electronic Imaging Systems (CEIS), a Center for Advanced Technology (CAT) supported by the New York State Office of Science, Technology & Academic Research (NYSTAR). The silicon PIN arrays were funded by a grant from NASA. The InSb arrays were also funded by NASA. Carnegie Observatories provided open-source hardware and software. The Space Telescope Science Institute's pyFits and numarray modules for Python were used extensively for the collection and analysis of data. The authors would like to thank all the team members at Raytheon Vision Systems for producing these fine multiplexers and hybridized focal plane arrays.

REFERENCES

1. A. C. Moore, Z. Ninkov, W. J. Forrest, C. McMurtry, G. S. Burley, and L. Avery, "Operation and test of Hybridized Silicon p-i-n Arrays using Open-source Array Control Hardware and Software," in *Proc. SPIE, Sensors and Camera Systems for Scientific, Industrial, and Digital Photography Applications IV*, M. M. Blouke, N. Sampat, and R. J. Motta, eds., **5017**, pp. 240–253, Jan. 2003.
2. L. Mortara and A. Fowler, "Evaluations of CCD: Performance for Astronomical Use," *Proc. SPIE, Solid State Imagers for Astronomy* **290**, pp. 28–30, 1981.
3. B. Pain and B. Hancock, "Accurate Estimation of Conversion Gain and Quantum Efficiency in CMOS Imagers," in *Proc. SPIE, Sensors and Camera Systems for Scientific, Industrial, and Digital Photography Applications IV*, M. M. Blouke, N. Sampat, and R. J. Motta, eds., **5017**, pp. 94–103, Jan. 2003.
4. H. Holloway, "Collection Efficiency and Crosstalk in Closely Spaced Photodiode Arrays," *Journal of Applied Physics* **60**, pp. 1091–1096, 1986.
5. D. T. Cheung, "MTF Modeling of Backside-Illuminated PV Detector Arrays," *Infrared Physics* **21**, pp. 301–310, 1981.
6. V. I. Blynskii, A. Y. Kulikov, S. Y. Rakhley, and V. I. Osinskii, "Photoelectric Crosstalk between Silicon Photoelements," *Physica Status Solidii* **121**, pp. 227–233, 1990.
7. M. Rabbani, R. Shaw, and R. Van Metter, "Detective Quantum Efficiency of imaging systems with amplifying and scattering mechanisms," *J. Opt Soc. Am A* **4 (5)**, pp. 895–901, May 1987.
8. M. Davis, M. Greiner, J. Sanders, and J. Wimmers, "Resolution Issues in InSb Focal Plane array system design," *Proc SPIE, Conf on IR Detectors and Focal Plane arrays V* **3379**, pp. 288–299, 1998.
9. I. Brouk, Y. Nemirovsky, S. Lachowicz, E. A. Gluszak, S. Hinckley, and K. Eshraghian, "Characterization of crosstalk between CMOS photodiodes," *Solid State Electronics* **46**, pp. 53–59, 2001.
10. J. D. Gaskill, *Linear Systems, Fourier Transforms, and Optics*, John Wiley and Sons, New York, 1978.
11. R. Shaw, "The equivalent quantum efficiency of the photographic process," *J. Phot. Sci.* **11**, pp. 199–204, 1963.
12. A. C. Moore, "Theoretical and Practical System Aspects of Hybridized Array Control." Ph.D. dissertation, Rochester Institute of Technology Center for Imaging Science, to be published.
13. K. Ennico, M. McKelvey, C. McCreight, R. McMurray, R. Johnson, A. W. Hoffman, P. Love, and N. Lum, "Large Format Si:As IBC Array Performance for NGST and Future IR Space Telescope Applications," in *Proc. SPIE, IR Space Telescopes and Instruments*, J. C. Mather, ed., **4850**, pp. 890–901, 2002.
14. C. W. McMurtry, W. J. Forrest, A. C. Moore, and J. L. Pipher, "Next Generation Space Telescope: NIR InSb Array Development," in *Proc. SPIE, IR Space Telescopes and Instruments,*, J. C. Mather, ed., **4850**, pp. 847–857, Aug. 2002.
15. C. W. McMurtry, W. J. Forrest, A. C. Moore, and J. L. Pipher, "James Webb Space Telescope: Characterization of flight candidate NIR InSb Array," in *Proc. SPIE, Focal Plane Arrays for Space Telescopes,*, J. C. Mather, ed., **5167**, p. these proceedings, Aug. 2003.